Estimation of Aerodynamic and Control Derivatives of Small Fixed-Wing Aircraft using Numerical Simulations and Wind Tunnel Experiments

Carlos Alberto Almeida Seixas
carlosseixas@tecnico.ulisboa.pt

Instituto Superior Técnico, Universidade de Lisboa, Portugal

November 2022

Abstract

In recent years, the use of small UAVs (Unmanned Aerial Vehicles) in recreational and commercial activities has experienced significant growth. The benefits of UAVs mainly come from their high autonomy using automatic guidance and control systems. The performance of such systems depends a lot on the quality of the identified aircraft model, which becomes extremely important for the general process. The objective of this Thesis is to establish the necessary steps for the conception of a UAV, building a new model in XFLR5 "Test Aircraft" and completely recreating the model physically elaborated for analysis in the Wind Tunnel, so it is possible to compare the results for validation of the themselves, making it possible to analyze any model, so that it is possible to build the identification of the model, incorporating analytical estimates and respective numerical simulations. It will be followed by wind tunnel tests. In the first instance, the aerodynamic and control derivatives will be determined to be used in simplified equations of longitudinal and lateral motion using analytical approximations. Found in the base literature for the present activity. Later, using available numerical tools, such as XFLR5 or Start-CCM+, best estimates are calculated based on a more detailed geometric definition of the UAV selected for the case study. Finally, a preliminary UAV model is identified, which can be validated in a wind tunnel.

Keywords: UAV, Aerodynamic Derivatives, Control Derivatives, Flight Stability and Flight Control.

1. Introduction

Analyse an aircraft it is a very complex procedure, we have a lot of tools to help analyse them and create then, systems engineering is one of the most used technique in engineering fields such as control engineering, industrial engineering, and interface design, to deal with the complex projects.

In more detail the study model of the master's thesis "Test Aircraft" goes through the construction of a simple model in CFD-XFLR5, to later replicate its characteristics, building a real model of "Test Aircraft", completely equal to the virtual model to analyze in the Wind Tunnel.

2. Background

2.1. Numerical Models

A numerical model is a combination of a large number of mathematical equations that depends upon computers to find an approximate solution to the underlying physical problem. Using the first few terms of a Taylor Series to get an approximate value for a function.

Taylor series is the series of functions of the form [1]:

$$f(x) = \sum_{n=0}^{\infty} a_n (x-a)^n \qquad \text{since} \qquad a_n = \frac{f^n(a)}{n!} \quad (1)$$

Where $f(x)$ is a given analytic function. In this case, the series above is said to be the Taylor series of $f(x)$ around the point $x = a$. Associated, the Taylor polynomial of order n around $x = a$ of a given n-times differentiable function at this point is given by[4]:

$$p(x) = f(a) + f'(a)\frac{(x-a)^1}{1!} + ... + f^n(a)\frac{(x-a)^n}{n!} \quad (2)$$

To better estimate the stability derivatives will be use the method of finite [5] difference that is a mathematical expression of the form $f(x+b) - f(x+a)$. If a finite difference is divided by $b - a$, one gets a difference quotient. The approximation of derivatives by finite differences plays a central role in finite difference methods for the numerical solution

of differential equations, especially boundary value problems.

The difference operator, commonly denoted Δ is the operator that maps a function f to the function $\Delta|f|$ defined by [8]:

$$\Delta|f|(x) = f(x+1) - f(x)\Delta|f|(x) = f(x+1) - f(x) \tag{3}$$

A difference equation is a functional equation that involves the finite difference operator in the same way as a differential equation involves derivatives. There are many similarities between difference equations and differential equations, specially in the solving methods. Certain recurrence relations can be written as difference equations by replacing iteration notation with finite differences.

In numerical analysis, finite differences are widely used for approximating derivatives, and the term "finite difference" is often used as an abbreviation of "finite difference approximation of derivatives". Finite difference approximations are finite difference quotients in the terminology employed above [7].

$$f'(x) = \frac{f(x+\Delta x) - f(x)}{\Delta x} + O(\Delta x) \tag{4}$$

$$f'(x) = \frac{f(x+\Delta x) - f(x-\Delta x)}{2\Delta x} + O(\Delta x^2) \tag{5}$$

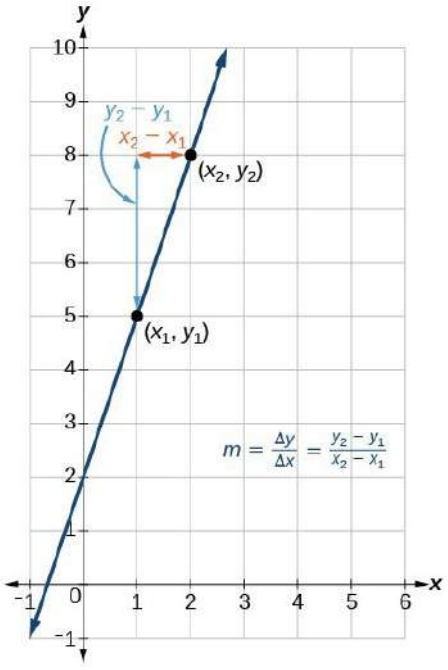

Figure 1: Finite Difference

2.2. Identification of Relevant Stability Derivatives

Stability derivative measures how much change occurs in a force or moment acting on the vehicle when there is a small change in a flight condition parameter such as angle of attack, airspeed, altitude.

2.2.1 For Longitudinal Model

In order to obtain the equations describing longitudinal vehicle motions, we need to be able to evaluate all the coefficients. This means we need to be able to provide estimates for the derivatives of X Force, Z Force, and M Moment, with respect to the relevant independent variables u velocity, w angular velocity, and q pitch rate. These stability derivatives usually are expressed in terms of dimensionless aerodynamic coefficient derivatives. [9]

Longitudinal dimensional derivatives:

$$X_u = \frac{1}{2}\rho u_0 S C_{x_u} \quad Z_u = \frac{1}{2}\rho u_0 S C_{z_u} \quad M_u = \frac{1}{2}\rho u_0 \bar{c} S C_{m_u}$$
$$X_w = \frac{1}{2}\rho u_0 S C_{x_\alpha} \quad Z_w = \frac{1}{2}\rho u_0 S C_{z_\alpha} \quad M_w = \frac{1}{2}\rho u_0 S \bar{c} C_{m_\alpha}$$
$$X_q = \frac{1}{4}\rho u_0 S \bar{c} C_{x_q} \quad Z_q = \frac{1}{4}\rho u_0 S \bar{c} C_{z_q} \quad M_q = \frac{1}{4}\rho u_0 S \bar{c}^2 C_{m_q}$$

2.2.2 For Lateral Model

In order to obtain the equations describing lateral/directional vehicle motions, we need to be able to evaluate all the coefficients. This means we need to be able to provide estimates for the derivatives of Y Force, L Moment, and N Moment, with respect to the relevant independent variables v angular velocity, p roll rate, and r yaw rate. As for the longitudinal case, these stability derivatives usually are expressed in terms of dimensionless aerodynamic coefficient derivatives. [9]

Lateral dimensional derivatives:

$$Y_v = \frac{1}{2}\rho u_0 S C_{y_\beta} \quad Y_p = \frac{1}{4}\rho u_0 S b C_{y_p} \quad Y_r = \frac{1}{4}\rho u_0 S b C_{y_r}$$
$$L_v = \frac{1}{2}\rho u_0 S b C_{l_\beta} \quad L_p = \frac{1}{4}\rho u_0 S b^2 C_{l_p} \quad L_r = \frac{1}{4}\rho u_0 S b^2 C_{l_r}$$
$$N_v = \frac{1}{2}\rho u_0 S b C_{n_\beta} \quad N_p = \frac{1}{4}\rho u_0 S b^2 C_{n_p} \quad N_r = \frac{1}{4}\rho u_0 S b^2 C_{n_r}$$

The estimation of aerodynamic derivatives from flight test measurements is an established and well developed experimental process. However, derivative estimates are usually obtained indirectly since it is not possible to measure the aerodynamic components of force and moment acting on the airframe directly. Also, since the aircraft has six degrees of freedom, it is not always possible to perturb the single motion variable of interest without perturbing some, or all, of the others as well. However, as in wind tunnel testing, some derivatives are easily estimated from flight test experiments with a good

degree of confidence, whereas others can be notoriously difficult to estimate.

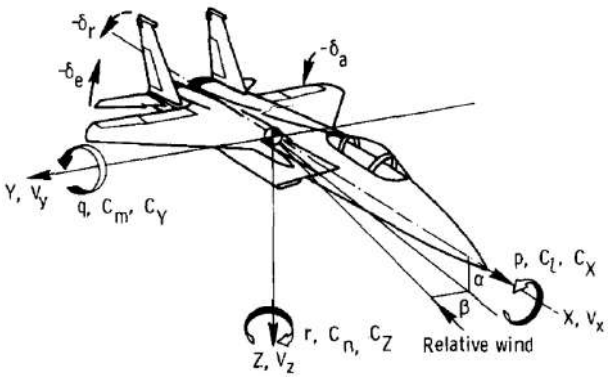

Figure 2: Model Characterization - Official Axes Reference

2.3. Control Derivatives of Linearized Equations

Control derivative measures how much change occurs in a force or moment acting on the vehicle when there is a small change in the deflection of a control surface such as the ailerons, elevator, and rudder.

The control derivatives consist of the pitching moment due to elevator deflection δ_e .

$$M_{\delta_e} = \frac{\frac{1}{2}\rho V^2 S\bar{c}}{I_y} C_{m\delta_e} \tag{6}$$

The rolling moment due to aileron deflection δ_a

$$L_{\delta_a} = \frac{\frac{1}{2}\rho V^2 Sb}{I_x} C_{l\delta_a} \tag{7}$$

And the yawing moment due to rudder deflection δ_r

$$N_{\delta_r} = \frac{\frac{1}{2}\rho V^2 Sb}{I_z} C_{n\delta_r} \tag{8}$$

There also can be significant cross-coupling of the rudder and aileron control moments, the yawing moment due to aileron deflection .

$$N_{\delta_a} = \frac{\frac{1}{2}\rho V^2 Sb}{I_z} C_{n\delta_a} \tag{9}$$

Is called adverse yaw, since this derivative usually is negative, leading to a tendency to rotate the nose to the left when the vehicle rolls to the right. The rolling moment due to rudder deflection.

$$L_{\delta_r} = \frac{\frac{1}{2}\rho V^2 Sb}{I_x} C_{l\delta_r} \tag{10}$$

Also tends to be unfavorable, as it tends to roll the vehicle to the left when trying to turn to the right.

2.4. Longitudinal Derivatives

The longitudinal aerodynamic coefficients acts in the plane which is called pitch plane and affected by the Lift force L, Drag force D, and pitch moment m. The effectiveness of these forces and moments are measured by lift coefficient C_L, drag coefficient C_D, and pitch moment coefficient C_m. These coefficients influenced by the angle of attack α, pitch rate q, and elevator deflection δ_e, but they are nonlinear in the angle of attack. For small α, our reference speed, the flow over the wings remain laminar, so no stall conditions will be happened, then we will linearize the equations about this linear zone.

Some non dimensional Derivatives can be analytically estimated as:

$$\begin{aligned} C_{x_u} &= C_{T_u} - C_{D_u} & C_{z_u} &= -C_{L_u} \\ C_{x_\alpha} &= C_{L_1} - C_{D_\alpha} & C_{z_\alpha} &= -(C_{L_\alpha} + C_{D_1}) \\ C_{z_{\dot{\alpha}}} &= -C_{L_{\dot{\alpha}}} & C_{z_q} &= -C_{L_q} \end{aligned}$$

$$\begin{cases} C_x = C_T + C_L\alpha_x - C_D \\ C_z = -(C_L + C_D\alpha_x) \end{cases} \tag{11}$$

$$\begin{cases} C_{T_u} = -2C_{T_0} \\ C_{T_u} = -3C_{T_0} \\ C_{T_0} = C_{D_1} + C_{W_0}\sin\theta_0 \end{cases} \tag{12}$$

$$\begin{cases} (C_{L_q})_{Tail} = 2V_H a_t \\ (C_{m_q})_{Tail} = -2V_H a_t \frac{l_t}{\bar{c}} \end{cases} \tag{13}$$

$$\begin{cases} (C_{L_q})_{Foil} \approx -2C_{L_\alpha}(h - h_0) \\ (C_{m_q})_{Foil} = \bar{C_{m_q}} - 2C_{L_\alpha}(h - \bar{h})^2 \end{cases} \tag{14}$$

2.5. Lateral Derivatives

The lateral aerodynamic coefficients of motion which is responsible of the yaw and roll motions. It's affected by the side force F_y, yaw moment n, and roll moment l. The effectiveness of these forces and moments are measured by side force coefficient C_y, yaw moment coefficient C_n, and roll moment coefficient C_n.

These coefficients influenced by sideslip angle , yaw angular rate r, roll angular rate p, aileron deflection δ_a, and rudder deflection δ_r, but they are nonlinear in these parameters.

All of these coefficients should be determined by wind tunnel. Linear approximations for these coefficients and their derivatives are acceptable for modeling purposes, the linearization is produced by the first-Taylor approximation, and non-dimensionalize of the aerodynamic coefficients of the angular rates.

Below are presented the equations that allow calculating each contribution of the dimensionless derivative, for the wing and for the tail, or for the sum of both contributions.

Tail contributions:

$$(C_{y_\beta})_{tail} = -a_F \left(1 - \frac{\partial\sigma}{\partial\beta}\right) \frac{S_F}{S} \tag{15}$$

$$(C_{y_p})_{tail} = -a_F \frac{S_F}{S} \left(\frac{2z_F}{b} - \frac{\partial\sigma}{\partial\hat{p}}\right) \tag{16}$$

$$(C_{y_r})_{tail} = a_F \frac{S_F}{S} \left(2\frac{l_F}{b} + \frac{\partial\sigma}{\partial\hat{r}}\right) \tag{17}$$

$$(C_{l_\beta})_{tail} \approx -a_F \frac{S_F z_F}{Sb} \left(1 - \frac{\partial\sigma}{\partial\beta}\right) \tag{18}$$

$$(C_{l_p})_{tail} \approx -a_F \frac{S_F}{S} \left(\frac{2z_F}{b} - \frac{\partial\sigma}{\partial\hat{p}}\right) \frac{z_F}{b} \tag{19}$$

$$(C_{l_r})_{tail} = a_F \frac{S_F}{S} \frac{z_F}{b} \left(2\frac{l_F}{b} + \frac{\partial\sigma}{\partial\hat{r}}\right) \tag{20}$$

$$(C_{n_\beta})_{tail} = a_F V_V \left(1 - \frac{\partial\sigma}{\partial\beta}\right) \tag{21}$$

$$(C_{n_p})_{tail} = a_F V_V \left(\frac{2z_F}{b} - \frac{\partial\sigma}{\partial\hat{p}}\right) \tag{22}$$

$$(C_{n_r})_{tail} = -a_F V_V \left(2\frac{l_F}{b} + \frac{\partial\sigma}{\partial\hat{r}}\right) \tag{23}$$

Wing contributions:

$$(C_{l_\beta})_{diedro} \approx -\frac{1+2\lambda}{6(1+\lambda)} a_0 \Gamma \tag{24}$$

$$(C_{l_\beta})_{offset} \approx -\frac{1+2\lambda}{3(1+\lambda)} C_l \tan\Lambda \tag{25}$$

$$(C_{l_\beta})_{wingposition} \approx \begin{cases} = -0.00016/^\circ \\ = 0 \\ = +0.00016/^\circ \end{cases} \tag{26}$$

$$(C_{l_p})_{wing} \approx -\frac{a_w}{12} \frac{1+3\lambda}{1+\lambda} \tag{27}$$

$$(C_{l_r})_{wing} \approx \frac{C_l}{6} \frac{1+3\lambda}{1+\lambda} \tag{28}$$

$$(C_{n_p})_{wing} \approx -\frac{C_l}{8} \tag{29}$$

3. Design and Building of Aircraft Models

3.1. Test Aircraft

The Test Aircraft main objective is, in scientific terms, to know with certainty the real profile type and also the model for CFD in order to be able to compare as realistically as possible the real model, with the virtual model analyzed in XFLR5. Thus, we can assure that the real model results obtained in the wind tunnel and also the virtual model in the XFLR5 are validate, because we know the distances, profiles, wingspan and all the characteristics of the aircraft both in reality and in the virtual model, being able to guarantee a correct and appropriate validation of the obtained results, as the recreated models are exactly the same.

Figure 3: Test Aircraft Wind Tunnel Assembly

3.2. Airfoil Profile Design

To choose the most suitable airfoil for the test model, it is necessary to make quantitative calculations to choose with accuracy the ideal airfoil for experimentation, considering reference values of aircraft speed V, kinematic viscosity ν and air density ρ, that can be seen in Table 1.

Table 1: Model Test Reference Values

V - Air Speed	20 m/s
ν - Kinematic Viscosity	1.51×10^{-5} m^2/s
ρ - Air Density	1.225 kg/m^3
AR - Aspect Ratio	8
b - Wingspan	1 m
g - Gravity Acceleration	9.81 m/s^2
W - Aircraft Mass	1.2 kg

3.2.1 Main Wing

The wing span $b = 1m$, was chosen because as the maximum allowed to be tested in the wind tunnel and also $AR = 8$ inspired on Cessna.

$$AR = \frac{b}{c} = 8 <=> 8 = \frac{1}{c} <=> c = 0.125m \tag{30}$$

Since the wing is rectangular, to make it as simple as possible, for better accuracy results, we obtain the wing area as.

$$S = b \times c = 1 \times 0.125 = 0.125m^2 \qquad (31)$$

When the UAV is in trimming fly, the Lift is equal to Weight. So applying the general formula for the lift coefficient given by.

$$C_L = \frac{W}{\frac{1}{2}\rho V^2 S} \qquad and \qquad L = W \qquad (32)$$

Where V is aircraft speed, ρ air density, S surface area, c wing chord, b wing span, W weight of the UAV and L lift force, replacing the values we obtain the reference lift coefficient.

$$C_L = \frac{1.2 \times 9.81}{\frac{1}{2} \times 1.225 \times 20^2 \times 0.125} = 0.384 \qquad (33)$$

We calculate the reference Reynolds number by.

$$Re = \frac{Vc}{\nu} = \frac{20 \times 0.125}{1.51 \times 10^{-5}} = 165562.9139 \qquad (34)$$

So now having the Reynolds and Lift Coefficient reference values, it is possible to chose the best low Reynolds number airfoil for the experience.

Analyzing between 2 low Reynolds numbers, we choose the profiles that best adapt to our case, this choice was made by the conventional low Reynolds number profiles [10]

The Selig/Donovan SD7062 low Reynolds number airfoil is shown in Figure 4.

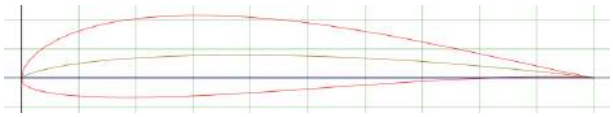

Figure 4: Profile SD7062 (14% Thickness)

The Selig S8036 low Reynolds number airfoil is shown in Figure 5.

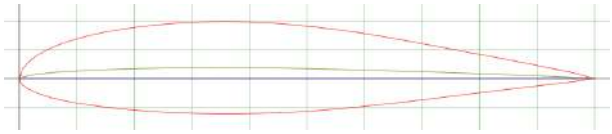

Figure 5: Profile S8036 (16% Thickness)

Then a comparison was made between the polar lines of the expected actuation range of Reynolds numbers, $Re = 165562.9$, consequently comparing between the lines of $Re = 100000$ and $Re = 200000$, between the two proposed 2D profiles, with the objective of verifying which of the two would have a lower drag coefficient for the expected lift coefficient.

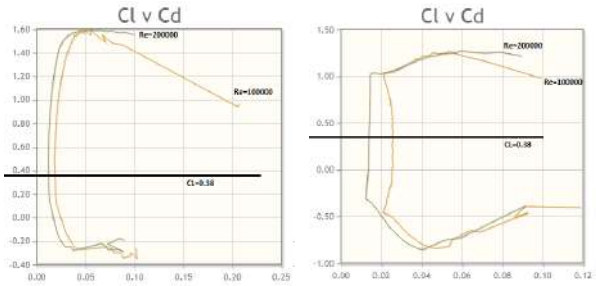

(a) SD 7062 (b) S 8036

Figure 6: C_L vs C_D Polars for $Re = 100000$ and $Re = 200000$

As we can see in the Figure 6, drawing a horizontal line at $C_L = 0.38$, at the intersection of the line with the polar lines of the respective Reynolds number, we observe that between the two chosen profiles, the one that presents the lowest drag coefficient is the **SD 7062** profile, so we can conclude that it is the most efficient profile for the chosen reference flight conditions, so this will be the design profile chosen for the Test Aircraft Model.

3.2.2 Tail and Fin Airfoil

For the tail wing and vertical fin, a symmetrical profile more suitable for low Reynolds numbers was chose, which will be the **NACA 0015** profile, illustrated in Figure 7. [10]

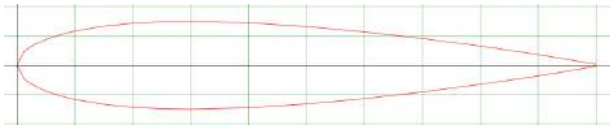

Figure 7: Profile NACA 0015

The NACA 0015 airfoil is symmetrical, the 00 indicating that it has no camber. The 15 indicates that the airfoil has a 15% thickness to chord length ratio: it is 15% as thick as it is long.

3.3. F35 Aircraft

The F35 Aircraft was specially designed for the present master's thesis. It is a replica of the F35 Fighter,, the "Open Source" design project, available online [1] , was used for the design base, however many changes were made in order to aesthetic

[1] By Julius Perdana 2020 Webpage

and mainly aerodynamic improvements, in order to maximize its load capacity and efficiency.

Figure 8: F35 Aircraft Wind Tunnel Assembly

In the master's thesis, the construction process and design, of both "Test Aircraft" and "F35 Aircraft" is detailed reported, as well as the procedure, materials used and construction method.

4. Calibration of Force Balance

Regarding the calibration process, when it came to simple, pure forces, only in one direction, a weight of 5N was added every 30 seconds. Initially, for 30 seconds, the scale was left without any weight just to stabilize the bars, then every 30 seconds 5N of weight were added, until we get 25N of total weight.

(a)

(b)

Figure 9: Force and Moment Calibration Process

In the figure 10 we can see the example of the results measured when the known loads were applied along the positive Fx axis. Each level of the graph corresponds to a new load of 5N applied, and the horizontal distance of the new level, corresponds to 30 seconds of waiting to stabilize the values and have a stable reading of the results.

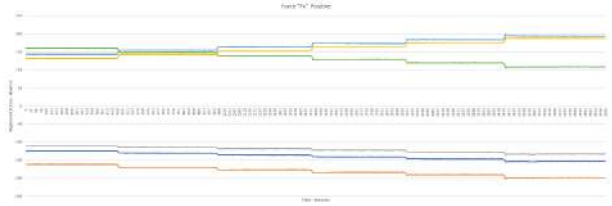

Figure 10: Calibration Results for Force "Fx" Positive

In figure 11, calibration assignments were made for combined forces and moments, with the same time interval of 60 seconds, and force interval of 0N, 5N, 10N, 15N, 20N and 25N, at the same time in all forces studied in the case. Thus, we obtain a more realistic reading of the expected values, as well as their influence between the bars for the various configurations of forces and moments applied.

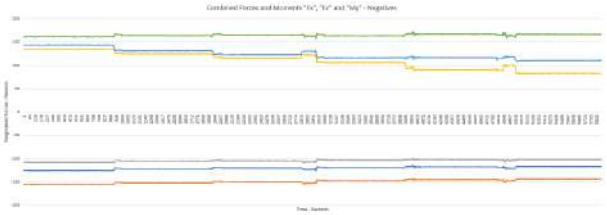

Figure 11: Calibration Results for Combined Forces and Moments "Fx", "Fz" and "My" Negative

This is the closest example of the reality of an aircraft in which several forces and moments of different values interact on the aircraft body, lift forces, drag forces, weight forces and trust forces. To produce the binary we apply forces with a $20cm$ distance, in every axes. It is important to mention that, in the conjugated forces, as I only have two arms, and it was necessary to change the weights in 3 places at the same time, so, there were small oscillations in the load/weight transitions, however, the results of these oscillations have been excluded to not affect the accurate calibration.

5. Implementation

5.1. Test Aircraft

5.1.1 CFD - XFLR5

The following results were obtained for the distribution of the Pressure Coefficient C_p along the surface of the supporting wings, in which the red represents the Pressure Coefficient with the highest value, positive pressure coefficient which implies value above atmospheric pressure and the blue represents the value of the lowest Pressure Coefficient, negative pressure coefficient which implies value below atmospheric pressure, in Figures 12 to 13. [2]

Comparing the results from Figure 12 to 13 the process that the greater the angle of attack, the lower the pressure coefficient on the upper surface of the airfoil, since the analysis was performed with viscous fluid, in Real Fluid due to an angle of attack increase, imply that the "micro turbulence" inside the boundary layer close to the airfoil upper surface will increase, until the point that the boundary layer of the flow detaches from the upper surface of the airfoil and the body becomes in a non-fuselated body, due to the excessive increase in the angle of attack and, consequently, the separation of the boundary layer from the upper surface of

the airfoil occurs, creating stall, but since the calculation and study was performed to small angles of attack $-2° < \alpha < 3°$, we will not have boundary layer separation, however, we show the analysis to $\alpha < 11°$, just for information proposes.

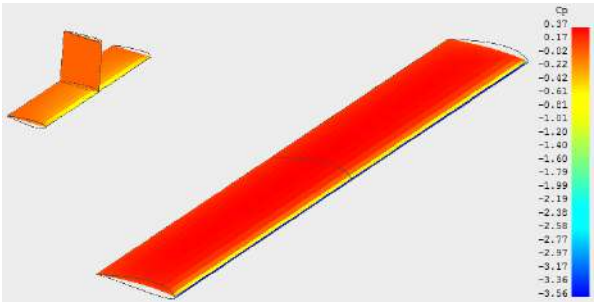

(a) $\alpha = -2°$

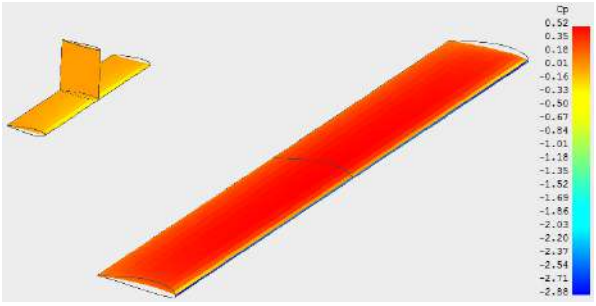

(b) $\alpha = 0°$

Figure 12: C_p Distribution for Angles of Attack $\alpha = -2°$ and $\alpha = 0°$

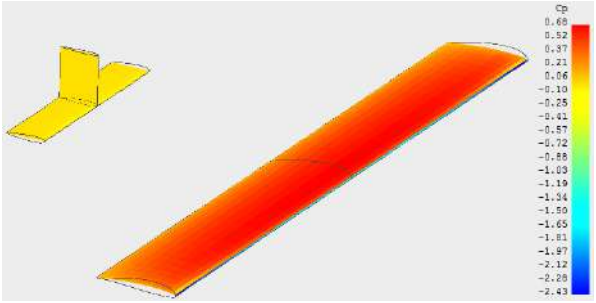

(a) $\alpha = 1.5°$

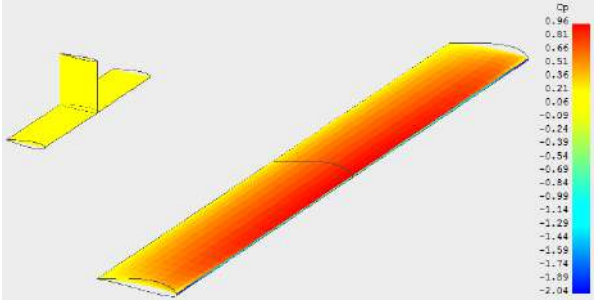

(b) $\alpha = 3°$

Figure 13: C_p Distribution for Angles of Attack $\alpha = 1.5°$ and $\alpha = 3°$

It is very important to emphasize that this analysis of the UAV was carried out in viscous fluid analysis, in what is called Real Fluid, in Perfect Fluid inviscid fluid it would be different since we never experience boundary layer separation and we will always have zero drag as long as the body is closed. [3]

In the following graphs present in Figure 14 we can observe the variations of the different aerodynamic coefficients, with the variation of the angle of attack between $-2° < \alpha < 11°$.

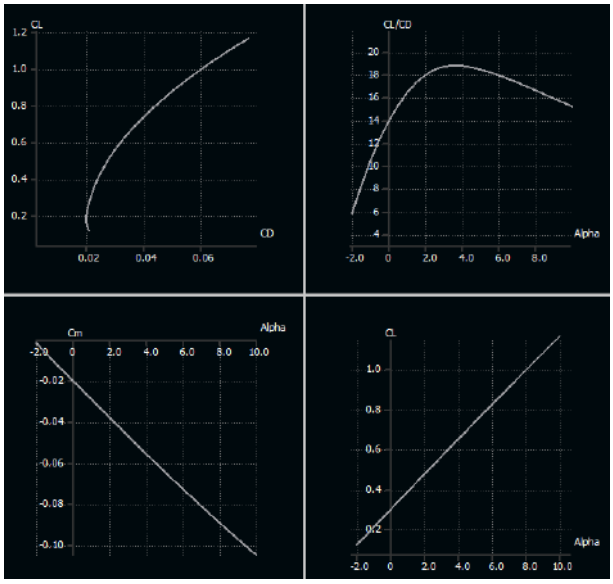

Figure 14: 3D Graphics C_L vs C_D ,C_L/C_D vs α, C_m vs α and C_L vs α with variation of $-2° < \alpha < 11°$

5.1.2 Wind Tunnel

In this chapter, the process of collecting data from the experiment is presented, in order to obtain the results with the greatest possible consistency.

Figure 15: Test Aircraft Geometry and Inertia Distribution

In Figure 15 it is possible to observe the installed set up, the aircraft model under analysis as well as the force balance fixed in the wind tunnel.

In this experiment, the forces are being measured with certainty at the base of the balance, precisely in each of the bars, and after the calibration process, the axial force equations of each bar were calculated in order to interpret their interaction, thus calculating forces measured at the base of the balance.

It is only necessary to estimate the value of C_D through empirical formulas, because it is not possible to calculate the C_D on the balance, it is a value that will have to be approximately calculated.

This is just an example of the observed reference values, air velocity equal zero, reference values were always observed before starting the wind tunnel, later, an arithmetic average was calculated due to the oscillations observed in the figure 16, to determine the average reference value , to later be subtracted from the average value of the results obtained with the wind tunnel in operation. [6]

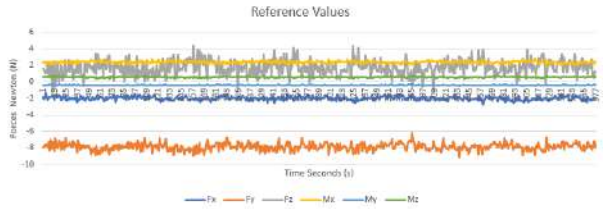

Figure 16: Reference Wind Tunnel Values - 2 minutes

As previously mentioned, the average values of the observed readings were calculated for each of the measured forces, with the action of the wind tunnel, it is possible to observe the results obtained in the Table 2 and 3.

Table 2: Test Aircraft - Forces Mean Values

	$F_x(N)$	$F_y(N)$	$F_z(N)$
Reference	-1.9914426	-7.8532205	1.7368939
6.3 m/s	-2.4930362	-5.4903101	-0.6614839
10 m/s	-3.2440922	-3.7034423	-3.1889875
15 m/s	-3.9121159	-1.6561105	-5.3802852

Subsequently, the difference between the value measured by the reference value was calculated, this difference is the correct value of the forces read on the scale for the different flight configurations.

Afterwards, it is necessary to calculate the Aerodynamic Lift and Pitch Coefficients of the respective forces.

Table 3: Test Aircraft - Moments Mean Values

	$M_x(N.m)$	$M_y(N.m)$	$M_z(N.m)$
Reference	2.3938353	-0.4106173	0.5910726
6.3 m/s	1.8437092	-0.3549904	0.8142319
10 m/s	1.5205711	-0.2578103	1.00309
15 m/s	0.9113611	0.0430932	0.8452989

$$C_L = \frac{L}{\frac{1}{2}\rho S V^2} \tag{35}$$

$$C_m = \frac{M}{\frac{1}{2}\rho S \bar{c} V^2} \tag{36}$$

Table 4: Test Aircraft - Aerodynamic Coefficients

Velocity	C_L	C_m
6.3 m/s	0.313257517	-0.058124423
10 m/s	0.643380434	-0.15966772
15 m/s	0.929590744	-0.474081172

To calculate the Drag Coefficient, it was necessary to use empirical expressions taking into account the 2 dimensions Drag Coefficient (2D) and 3 dimensions Drag Coefficient (3D),

$$C_{D_{3D}} = C_{D_{2D}}^{Friction} + C_{D_{2D}}^{Pressure} + C_{D_{3D}}^{InducedDrag} \tag{37}$$

Admitting pressure gradient equal zero, $C_{D_{2D}}^{Pressure} = 0.004$, elliptical circulation distribution and also leading edge transition,

$$C_{D_{3D}} = 2 \times 0.074 \times (R_e)^{-0.2} + 0.004 + \frac{C_L^2}{\pi \times 8} \tag{38}$$

Using the appropriate empirical formulas it is possible to calculate the Reynolds Number and the Drag Coefficient, presented in the following Table 5,

Table 5: Test Aircraft - Aerodynamic Coefficients

Velocity	R_e	C_D
6.3 m/s	52152.31788	0.024762516
10 m/s	82781.45695	0.035840129
15 m/s	124172.1854	0.052555835

5.2. **F35 Aircraft**

5.2.1 Wind Tunnel

In the previous chapter of calculating the stability derivatives for "Test Aircraft", the values were first calculated in CFD and later we obtained their validation in the Wind Tunnel, taking advantage of this verification we can calculate with certainty the derivatives in the "F35 Aircraft" with great certainty of the results obtained without their validation in CFD.

Figure 17: F35 Aircraft in Wind Tunnel

Here, we use the same process described in section 5.1.2 in the Wind Tunnel subsection. Exactly the same procedure, however without having the validation comparison previously made between the CFD and the Wind Tunnel for Test Aircraft. In Table 6, the values of C_L and C_m obtained in the balance of forces are presented.

Table 6: F35 Aircraft - Aerodynamic Coefficients

Velocity	C_L	C_m
6.3 m/s	0.293236093	-0.100281345
10 m/s	0.315918853	-0.081049705
15 m/s	0.334786727	-0.044046167

Using the values read on the force balance of C_L and C_m, it is possible to calculate the Reynolds number, and with these three values of aerodynamic coefficients it is possible to estimate the value of the Drag Coefficient C_D, using the same process and formulas and the same assumptions assumed in the Test Aircraft, elliptical circulation distribution, leading edge transition, pressure gradient equal to zero, and $C_{D_{2D}}^{Pressure} = 0.004$. In Table 7 it´s possible to see the final calculated values.

Table 7: F35 Aircraft - Aerodynamic Coefficients

Velocity	R_e	C_D
6.3 m/s	108476.8212	0.021982435
10 m/s	172185.4305	0.021246957
15 m/s	258278.1457	0.020701376

In Figure 18, it is possible to observe the variations of the forces according to the increase in speed of the aircraft, as well as their changes of level according to the increase of the speed, they were stabilized for two minutes to calculate an average of all the values read for a correct reading after each speed. Each color represents a force, the most relevant being the gray color that represents "F_z" and consequently the Lift, the axis system being considered that makes the "F_z" axis is positively directed towards the ground, and the more negative the value of "F_z" greater Lift is generated.

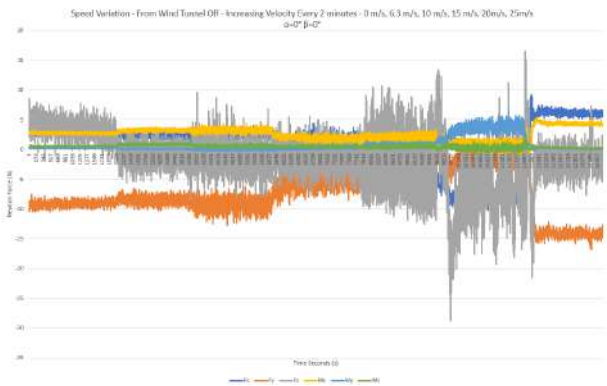

Figure 18: F35 Aircraft Speed Variation - 0 m/s, 6.3 m/s, 10 m/s, 15 m/s, 20m/s, 25m/s, 0 m/s

6. Results

Table 8: Test Aircraft - XFLR5

Longitudinal		Lateral	
X_u	0.0020	Y_v	-0.0027
X_w	0.2274	Y_p	-0.0004
X_q	0.0037	Y_r	0.0011
Z_u	0	L_v	-0.0005
Z_w	-0.0926	L_p	-0.0051
Z_q	-0.0037	L_r	0.0001
M_u	8.27E-6	N_v	0.0011
M_w	-0.0008	N_p	0.0001
M_q	-0.0015	N_r	-0.0004

Table 9: Test Aircraft - Wind Tunnel

Longitudinal		Lateral	
X_u	-0.0024	Y_v	-0.0069
X_w	0.6982	Y_p	N/A
X_q	N/A	Y_r	N/A
Z_u	-0.0542	L_v	-0.0294
Z_w	-0.3565	L_p	N/A
Z_q	N/A	L_r	N/A
M_u	-0.0045	N_v	-0.0023
M_w	-0.0087	N_p	N/A
M_q	N/A	N_r	N/A

Table 10: Stability Derivatives F35 Aircraft - Wind Tunnel

Longitudinal		Lateral	
X_u	0.0003	Y_v	-0.0236
X_w	0.4257	Y_p	N/A
X_q	N/A	Y_r	N/A
Z_u	-0.0098	L_v	-0.1056
Z_w	-0.1249	L_p	N/A
Z_q	N/A	L_r	N/A
M_u	0.0034	N_v	-0.0082
M_w	-0.0051	N_p	N/A
M_q	N/A	N_r	N/A

Table 11: Control Derivatives Test Aircraft

XFLR5		Wind Tunnel	
X_{δ_e}	-0.0008	X_{δ_e}	-0.0018
Y_{δ_r}	0.0084	Y_{δ_r}	0.0199
X_{δ_a}	0	X_{δ_a}	0.0022
Z_{δ_e}	-0.0568	Z_{δ_e}	-0.0510
L_{δ_r}	0	L_{δ_r}	0.0041
Z_{δ_a}	0	Z_{δ_a}	0.0083
M_{δ_e}	-0.0201	M_{δ_e}	0.0009
N_{δ_r}	-0.0004	N_{δ_r}	-0.0004
M_{δ_a}	0	M_{δ_a}	-0.0004

7. Conclusions

Since we use different methods, XFLR5 and Wind Tunnel, to estimate the aerodynamic derivatives, and in the end we obtain approximated values, it is a case to say that all the experience where successful, different model collectors and in the end practically the same results. After calculating the results in the XFLR5 and having them validated in the Wind Tunnel, it is clear that there is real and high confidence in the results obtained in the Wind Tunnel for the F35 Aircraft, knowing that the proximity obtained in Test Aircraft results, confirmed that the readings on the force balance are very realistic and coherent, with a high degree of accuracy. Since we obtain the values from different methods, XFLR5-CFD and Wind Tunnel, and in the end, they were really close values, which is an entirely satisfactory result, considering that different reading methods were used, CFD in a virtual reading model with a virtual model, creating a real model, recreated in full to be coupled to the scale of forces and obtain results in the Wind Tunnel, are incredible results.

References

[1] H. Auchter. *Brook Taylor, der mathematiker und philosoph; beiträge zur wissenschaftsgeschichte der zeit des Newton-Leibniz-streites.* Würzburg, K. Triltsch, 1937.

[2] V. Blacksburg. "about xflr5 calculations and experimental measurements,". *Presentation document*, 2009.

[3] V. de Brederode. *Aerodinâmica Incompressível: Fundamentos.* IST Press, 2^{nd} edition, Junho de 2018.

[4] E. C. de Oliveira. *Funções Especiais com Aplicações.* Editora Livraria da Fisica, , note = ISBN 8-588-32542-X edition.

[5] D. C. Fraser. *"On the Graphic Delineation of Interpolation Formulae".* Journal of the Institute of Actuaries, , note = 43 (2): 235–241 edition, January 1, 1909.

[6] N. Hall. *Force Balance.* National Aeronautics and Space Administration - NASA, 2021.

[7] F. Lessman. *Finite Difference Equations.* Springer, 1992. ISBN 0-486-67260-3.

[8] I. Newton. *Principia.* Lemma V, book iii edition, (1687).

[9] J. Oliveira. Apontamentos de estabilidade de voo. Instituto Superior Técnico, 2019.

[10] L. W. Traub and C. Coffman. Efficient low-reynolds-number airfoils. *JOURNAL OF AIRCRAFT*, page 17, 2019. DOI: 10.2514/1.C035515.